



## Generation of attosecond pulses with a controllable carrier-envelope phase via high-order frequency mixing

V. A. Birulia <sup>1</sup>, M. A. Khokhlova <sup>2,3,\*</sup> and V. V. Strelkov<sup>1,4</sup>

<sup>1</sup>*Moscow Institute of Physics and Technology (National Research University), Institutskiy per. 9, Dolgoprudny 141701, Russia*

<sup>2</sup>*Max Born Institute for Nonlinear Optics and Short Pulse Spectroscopy, Max-Born-Straße 2A, Berlin 12489, Germany*

<sup>3</sup>*King's College London, Strand, London WC2R 2LS, UK*

<sup>4</sup>*Prokhorov General Physics Institute of the Russian Academy of Sciences, Vavilova Street 38, Moscow 119991, Russia*



(Received 22 April 2022; revised 28 July 2022; accepted 2 August 2022; published 16 August 2022)

Advancing table-top attosecond sources in brightness and pulse duration is of immense interest and importance for an expanding sphere of applications. Recent theoretical studies [New J. Phys. **22**, 093030 (2020)] found that high-order frequency mixing (HFM) in a two-color laser field can be much more efficient than high-order harmonic generation (HHG). Here we study the attosecond properties of the coherent extreme ultraviolet (XUV) generated via HFM analytically and numerically, focusing on the practically important case when one of the fields has much lower frequency and much lower intensity than the other one. We derive simple analytical equations describing intensities and phase locking of the HFM spectral components. We show that the duration of attosecond pulses generated via HFM, while being very similar to that obtained via HHG in the plateau, is shortened for the cutoff region. Moreover, our study demonstrates that the carrier-envelope phase of the attopulses produced via HFM, in contrast to HHG, can be easily controlled by the phases of the generating fields.

DOI: [10.1103/PhysRevA.106.023514](https://doi.org/10.1103/PhysRevA.106.023514)

### I. INTRODUCTION

The introduction of laser technologies ignited an explosion in the study of light and its interaction with matter. One of the areas from this realm is attosecond physics [1–4]. In turn, the rapid expansion of attophysics and the conquest of progressively ultrafast processes has created a hunger for attosecond sources and their active development, resulting in steady progress [5–8]. However, there is still a high demand for further efforts dictated by the needs of a growing sphere of applications.

Currently available table-top attosecond sources are based on the generation of high-order harmonics of intense laser pulses during their interaction with a gaseous medium. A process similar to high-order harmonic generation (HHG) occurs when two fields (at least one of which is intense and therefore causes photoionization of the gas) generate high-order mixed-frequency components. This process is called high-order frequency mixing (HFM) [9–19].

The efficiency of the macroscopic HHG response is substantially limited by the phase matching of the process. Namely, the process is indissolubly connected to the photoionization of the medium, and the change in the refractive index due to the ionization leads to weaker phase matching [20]. This limitation can be significantly softened for the HFM process under a proper choice of frequencies of the generating fields [21–25], resulting in much longer propagation distances of the phase-matched generation (including the case when the second field has much weaker intensity and much lower

frequency than the fundamental) and thus to higher efficiency of the HFM [26,27]. This advantage defines the perspective of using the HFM process to design highly effective attosecond pulse sources. The scope of the current paper is the theoretical investigation of these perspectives.

In this paper we study theoretically the microscopic aspects of attosecond pulse generation via the HFM process. Our analytical approach is based on the strong-field approximation (SFA) [28] extended to include the second weak field perturbatively [29]. Assuming that this field can be considered as a quasistatic one, we derive simple analytical equations for the amplitudes and phases of the HFM components. The analytical SFA results are compared with ones of the numerically integrated SFA and also with results obtained via numerical simulation of the three-dimensional time-dependent Schrödinger equation (3D TDSE).

An intrinsic feature of the HHG atomic response is its frequency modulation, or the “attochirp” [30–33]. It defines the lower limit for the duration of the attosecond pulse in the plateau region [34]. Here we study the attochirp of the pulses obtained via HFM both for the plateau and the cutoff regions.

The phase of the carrier with respect to the pulse envelope, or the carrier-envelope phase (CEP), is a key feature of the few-cycle pulses. The ability to stabilize it via  $f$ - $2f$  interferometry [35] and to control it leads to numerous new perspectives in studies of the interaction of intense femtosecond pulses with matter. However, the CEP of the attosecond pulses obtained via HHG cannot be controlled easily. In this paper we show that HFM allows a straightforward way to control the CEP of the attosecond pulse via tuning the phases of the generating fields.

\*margarita.khokhlova@kcl.ac.uk

## II. ANALYTICAL THEORY

In this section we study analytically the microscopic response of a model atom to a two-color linearly polarized field in the framework of the strong-field approximation [28]. The two-color field consists of an intense laser field and a weaker low-frequency field which we assume for the moment to be static, so the total field is written as

$$E(t) = \mathcal{E}_0 \cos(\omega_0 t) + \mathcal{E}_1, \quad (1)$$

where the amplitudes of the strong field  $\mathcal{E}_0$  and of the weak field  $\mathcal{E}_1$  satisfy the condition

$$\mathcal{E}_1 \ll \mathcal{E}_0. \quad (2)$$

We write the time-dependent dipole moment derived as the integral (13) in Ref. [28] in the form

$$x(t) = \int_0^\infty d\tau f(t, \tau) \exp[-iS_{\text{st}}(t, \tau)] + \text{c.c.}, \quad (3)$$

where  $S_{\text{st}}(t, \tau)$  is the quasiclassical action and  $f(t, \tau)$  denotes the remaining part of the integrand excluding the exponent  $\exp(-iS_{\text{st}})$ .

The quasiclassical action is given as

$$S_{\text{st}}(t, \tau) = \frac{1}{2} \int_{t-\tau}^t dt'' [p_{\text{st}} - A(t'')]^2, \quad (4)$$

where

$$A(t) = -\frac{\mathcal{E}_0}{\omega_0} \sin(\omega_0 t) - \mathcal{E}_1 t \quad (5)$$

is the vector potential of the field (1) and  $p_{\text{st}}$  is the stationary value of the momentum, which allows the electron trajectory starting near the origin at the time instant  $t - \tau$  to return to the same position at the time instant  $t$ . This stationary value of the momentum in the field (1) is written as

$$p_{\text{st}} = p_{\text{st}}^{(0)} + (\tau/2 - t)\mathcal{E}_1, \quad (6)$$

where  $p_{\text{st}}^{(0)}$  is the stationary value of the momentum in the absence of the second field,<sup>1</sup> given by Eq. (14) in Ref. [28], which we rewrite in atomic units<sup>2</sup> as

$$p_{\text{st}}^{(0)} = \frac{\mathcal{E}_0}{\omega_0^2 \tau} [\cos(\omega_0 t) - \cos(\omega_0 t - \omega_0 \tau)]. \quad (7)$$

Substituting Eq. (6) in Eq. (4), we derive the action as

$$S_{\text{st}} = S_{\text{st}}^{(0)} - \frac{\mathcal{E}_1}{\mathcal{E}_0} \frac{2U_p}{\omega_0} D(t, \tau) + \frac{\mathcal{E}_1^2 \tau^3}{24}, \quad (8)$$

where

$$S_{\text{st}}^{(0)} = U_p \tau - \frac{2U_p}{\omega_0^2 \tau} [1 - \cos(\omega_0 \tau)] - \frac{U_p}{\omega_0} \cos[\omega_0(2t - \tau)] \left[ \sin(\omega \tau) - \frac{4 \sin^2(\omega_0 \tau/2)}{\omega_0 \tau} \right] \quad (9)$$

<sup>1</sup>Here and below we use the upper index <sup>(0)</sup> to denote values in the absence of the second field.

<sup>2</sup>Here we use standard atomic units in contrast to Ref. [28], where, in addition to the use of atomic units, all energies are expressed in terms of the laser photon energy.

is the action found in [28] for a single-color field,

$$D(t, \tau) = 2\{\sin[\omega_0(t - \tau)] - \sin(\omega_0 t)\} + \omega_0 \tau \{\cos(\omega_0[t - \tau]) + \cos(\omega_0 t)\} \quad (10)$$

and  $U_p = \mathcal{E}_0^2/4\omega_0^2$  is the ponderomotive energy in the strong field  $\mathcal{E}_0$ . Expression (8) presents the action in the field (1) with vector potential (5) as a quadratic polynomial in  $\mathcal{E}_1$ .

After expanding the exponent  $\exp(-iS_{\text{st}})$  up to the term proportional to  $\mathcal{E}_1^2$  within the new action (8), we obtain

$$\exp(-iS_{\text{st}}) = \exp(-iS_{\text{st}}^{(0)}) \left[ 1 + i \frac{\mathcal{E}_1}{\mathcal{E}_0} \frac{2U_p}{\omega_0} D(t, \tau) - \left( \frac{\mathcal{E}_1}{\mathcal{E}_0} \frac{2U_p}{\omega_0} \right)^2 D^2(t, \tau) \right], \quad (11)$$

where we neglect one of the two quadratic terms,  $i\mathcal{E}_1^2 \tau^3/24$  since it is dominated by the other one under the condition  $U_p/\omega_0 \gg 1$ .

In the limit where the ionization potential of the generating system is much smaller than the ponderomotive energy of the freed electron  $I_p \ll U_p$ , the integral (3) can be taken within the stationary point method as in Ref. [28]. The stationary point  $\tau = \tau_{\text{st}}(t)$  corresponds to the zero value of the initial velocity of the electron  $v(t - \tau) = p_{\text{st}}(t, \tau) - A(t - \tau) = 0$  for the quasiclassical action written in the form (4). Thus, the electron motion within this approximation is quasiclassical, and its features can be described within the simple-man picture [36,37]. Moreover, even if the condition  $I_p \ll U_p$  is not valid, the main contribution to the integral (3) is given by the vicinity of the point  $\tau = \tau_{\text{st}}$ , then the slowly varying function  $D(t, \tau)$  can be factored out from the integral as  $D(t, \tau_{\text{st}})$ . In this case from Eqs. (3) and (11) we can write the time-dependent dipole moment in the form

$$x(t) = x^{(0)}(t) + i \frac{\mathcal{E}_1}{\mathcal{E}_0} \frac{2U_p}{\omega_0} D[t, \tau_{\text{st}}(t)] x^{(0)}(t) - \left[ \frac{\mathcal{E}_1}{\mathcal{E}_0} \frac{2U_p}{\omega_0} D[t, \tau_{\text{st}}(t)] \right]^2 x^{(0)}(t). \quad (12)$$

The function  $x^{(0)}(t)$  changes its sign every half-cycle of the laser field, and thus its spectrum consists of odd harmonics [28]. From Eq. (10) we can see that function  $D[t, \tau_{\text{st}}(t)]$  also changes its sign every laser half-cycle. Therefore, the second term in Eq. (12) describes even harmonics and the third one describes the correction of the odd harmonics due to the static field.

If now we assume that the field  $\mathcal{E}_1$  is not a static one as in Eq. (1), but varies slowly with time

$$\mathcal{E}_1(t) = \mathcal{E}_1 \cos(\omega_1 t), \quad (13)$$

then for

$$\omega_1 \ll \omega_0 \quad (14)$$

it can be considered as a quasistatic field. If we change the static field  $\mathcal{E}_1$  in Eq. (12) with the quasistatic one (13), where  $\cos(\omega_1 t) = [\exp(-i\omega_1 t) + \exp(i\omega_1 t)]/2$ , this leads to the following alterations of the emitted spectrum. The linear term  $\propto \mathcal{E}_1$  causes the splitting of even harmonics into two satellites, shifted by  $\pm\omega_1$  from the harmonic frequencies. The

quadratic term  $\propto \mathcal{E}_1^2$ , meanwhile, results in the appearance of two satellites near the odd harmonics, shifted by  $\pm 2\omega_1$  from the harmonic frequencies, as well as a correction to the amplitude of the odd harmonics.

These spectral changes can be related to the nonlinear high-order frequency mixing processes involving  $q$  photons of the strong field  $\mathcal{E}_0(t)$  and  $m = 1, 2$  photons of the weak field  $\mathcal{E}_1(t)$  with an odd total number of photons  $q + m$ . Using the notations from Ref. [13], we describe these processes in terms of the induced susceptibilities  $\kappa_q^{(m)}$  defined as the ratio of the spectral component of the atomic response to the corresponding power of the weak field

$$\kappa_q^{(m)} \equiv x(\omega_2 = q\omega_0 + m\omega_1)/\mathcal{E}_1^{|m|}, \quad (15)$$

where  $x(\omega)$  is the spectrum of the atomic response  $x(t)$ . Under conditions (2) and (14),  $\kappa_q^{(m)}$  does not depend on either  $\mathcal{E}_1$  or  $\omega_1$  (see Ref. [13] for more details), but it does depend on  $\mathcal{E}_0$  and  $\omega_0$ . Thus, single-photon processes in the weak low-frequency field with the sum and difference frequencies are designated as  $m = 1$  and  $m = -1$ , respectively;  $m = 2$  and  $m = -2$  similarly denote two-photon processes.

The unperturbed harmonic response is denoted as  $\kappa_q^{(0)}$ :

$$\kappa_q^{(0)} \equiv \begin{cases} x^{(0)}(\omega_2 = q\omega_0), & \text{for odd } q, \\ (\kappa_{q-1}^{(0)} + \kappa_{q+1}^{(0)})/2, & \text{for even } q, \end{cases} \quad (16)$$

where  $x^{(0)}(\omega)$  is the spectrum in the absence of the second field.

Finally, the quadratic correction to the HHG response in the weak low-frequency field is described with the susceptibility

$$\kappa_q^{(0,2)} \equiv [x(\omega_2 = q\omega_0) - x^{(0)}(\omega_2 = q\omega_0)]/\mathcal{E}_1^2.$$

This susceptibility describes a two-photon process, but without a frequency change.

From Eq. (12) we derive the relative contributions of HFM processes in the two-color field in relation to the HHG process in the single-color field as

$$\frac{\kappa_q^{(\pm 1)}}{\kappa_q^{(0)}} = i \frac{U_p}{\mathcal{E}_0 \omega_0} D[t_q, \tau_{\text{st}}(t_q)], \quad (17)$$

$$\frac{\kappa_q^{(\pm 2)}}{\kappa_q^{(0)}} = - \left[ \frac{U_p}{\mathcal{E}_0 \omega_0} D[t_q, \tau_{\text{st}}(t_q)] \right]^2, \quad (18)$$

$$\frac{\kappa_q^{(0,2)}}{\kappa_q^{(0)}} = -2 \left[ \frac{U_p}{\mathcal{E}_0 \omega_0} D[t_q, \tau_{\text{st}}(t_q)] \right]^2. \quad (19)$$

Here  $t_q$  is the emission time of  $q$ th harmonic within the simple-man picture, i.e., the return time of the electron which starts from the origin with zero initial velocity and returns with kinetic energy corresponding to the emission of XUV with photon energy close to  $q\omega_0$ .

One can see from Eqs. (17) to (19) that contributions to the XUV spectrum involving one  $\mathcal{E}_1(t)$  field photon are shifted in phase by  $\pi/2$  with respect to the main contribution  $\kappa_q^{(0)}$ , while ones involving two photons are shifted by  $\pi$ . The latter can be understood as follows: The presence of the weak  $\mathcal{E}_1(t)$  field should not change the total XUV emission efficiency by much; thus, the appearance of the new spectral components with some intensities should lead to a *decrease* of the ‘‘main’’ spectral component (i.e., the one with  $m = 0$ ). Note that a

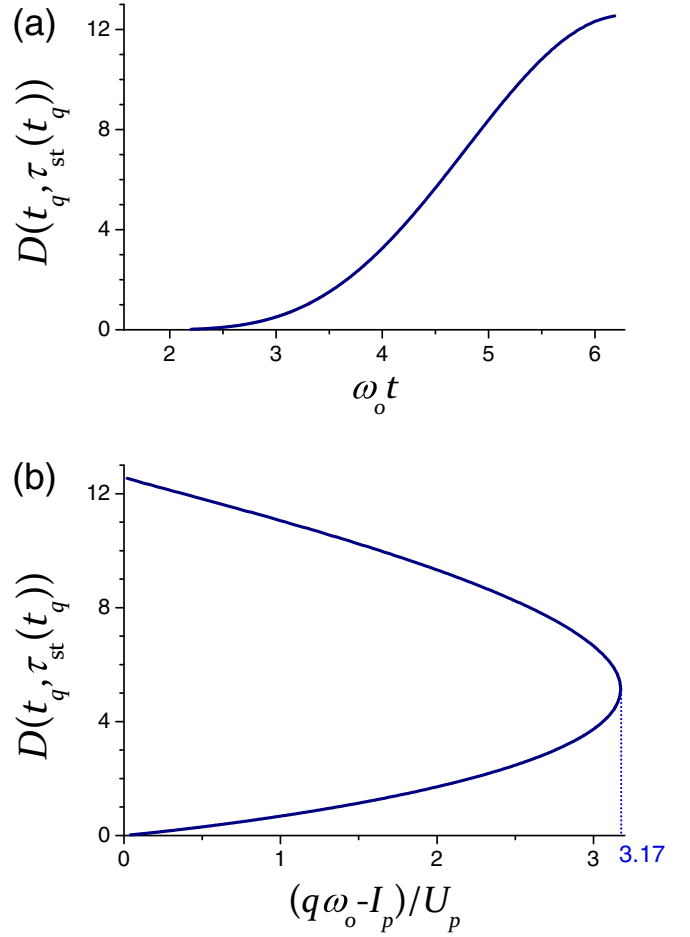


FIG. 1. The function  $D(t, \tau)$  (10) for the electron quasiclassical trajectory started from origin with zero initial velocity as a function of (a) the return time and (b) the returning electron kinetic energy divided by the ponderomotive energy.

recent study of above-threshold ionization has shown similar behavior of phase shifts for contributions involving different number of photons [38].

From Eqs. (17) to (19) we also see that the dependence of the induced susceptibilities on the laser parameters is given by the factor  $U_p/(\mathcal{E}_0 \omega_0) = \mathcal{E}_0/(4\omega_0^3)$ , while their dependence on the harmonic order is described by the function  $D[t_q, \tau_{\text{st}}(t_q)]$  calculated for the quasiclassical electron trajectory. Figure 1(a) presents the value of  $D[t_q, \tau_{\text{st}}(t_q)]$  as a function of the emission time and, in Fig. 1(b), of the harmonic order. For the long electronic trajectory, the  $D$  value is higher than for the short trajectory. This is natural because, the longer  $\tau$  is, the stronger the influence of the (quasi)static field on the electronic dynamics becomes.

Below, we consider only the short trajectory contribution because this is the one usually observed experimentally. For this contribution the susceptibilities grow with the harmonic order and this growth is more pronounced in the high-energy part of the plateau. Note that for the cutoff harmonics the assumption of a single quasiclassical trajectory is not valid (see, for instance, Ref. [39] and references therein). So for the cutoff harmonics the behavior of the susceptibilities could differ from one shown in Fig. 1.

At a certain “threshold” field amplitude  $\mathcal{E}_1^{\text{th}}$  the contributions of the processes of different orders become equal, i.e.,  $|\kappa_q^{(m)} \mathcal{E}_1^{\text{th}}| = |\kappa_q^{(m-1)}|$ . From Eqs. (17) to (19) we find this field as

$$\mathcal{E}_1^{\text{th}} = \mathcal{E}_0 \frac{\omega_0}{U_p D[t_q, \tau_{\text{st}}(t_q)]} = \frac{4\omega_0^3}{\mathcal{E}_0 D[t_q, \tau_{\text{st}}(t_q)]}. \quad (20)$$

Thus, if the laser field is intense (high  $\mathcal{E}_0$ ) and has low-enough frequency (low  $\omega_0$ ), the field  $\mathcal{E}_1$ , even if very weak, still provides relatively intense HFM components. We also would like to stress the strong dependence of  $\mathcal{E}_1^{\text{th}}$  on the laser field frequency ( $\propto \omega_0^3$ ).

For typical HHG conditions, namely, for laser-field intensity  $2 \times 10^{14} \text{ W/cm}^2$  and 800 nm wavelength, assuming  $D = 2$ , we find the threshold intensity of the weak field as low as  $8 \times 10^{11} \text{ W/cm}^2$ , which is  $4 \times 10^{-3}$  of the laser intensity. Note that this level of mid-IR and THz field intensity is currently rather achievable.

### III. HFM IN THE FREQUENCY DOMAIN

In this section we calculate spectral characteristics of the microscopic HFM response of a model argon atom in a two-color external field using numerically integrated SFA and numerical TDSE solution (“SFA” and “TDSE” below, respectively), and compare these results with the analytical theory, which we call “quasistatic SFA” or “qsSFA,” derived in the previous section for a quasistatic weak field. As above, here we consider the two-color field given by Eqs. (1) and (13) satisfying the conditions (2) and (14).

#### A. Methods

To find the nonlinear atomic response via full SFA, we calculate the integral (3) numerically using the code available in Ref. [40]. This approach allows one to separate different quantum path contributions for the plateau harmonics; here we study only the short quantum path contribution. Then we transform the time-dependent response to the spectral domain and use it to obtain the induced susceptibilities via Eq. (15). To obtain the nonlinear response from the TDSE, we solve the 3D TDSE via the numerical approach [41] for a single-active electron (SAE) atomic potential [42], modeling an argon atom in the two-color field.

In our simulations we use the same parameters of the external fields for SFA and TDSE calculations. The wavelength of the strong fundamental field is 1200 nm and its intensity is  $2.4 \times 10^{14} \text{ W/cm}^2$ . The frequency of the low-frequency field is  $\omega_1 = \omega_0/5$ . We would like to note that we checked that the results are almost not sensitive to  $\omega_1$  even at such (relatively high) values of this frequency. The intensity of the weak field is  $2.4 \times 10^9 \text{ W/cm}^2$  or  $10^{-5}$  of the strong field intensity. Thus the weak-field intensity is well below the threshold intensity in the range  $10^{10}$ – $10^{11} \text{ W/cm}^2$ , given by Eq. (20). The pulse duration is 105 fs, the pulse consists of 10 cycles  $\sin^2$  on-ramp, 20 cycles flat top, and 10 cycles  $\sin^2$  trailing edge.

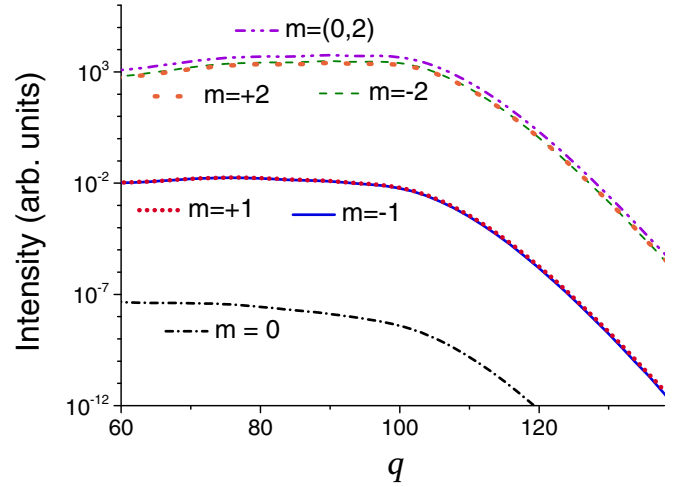


FIG. 2. Relative intensity of susceptibilities  $\kappa_q^{(m)}$  for HFM ( $m \neq 0$ ) and HHG ( $m = 0$ ) components as functions of the number of strong-field quanta  $q$  for processes involving different numbers of the weak low-frequency field quanta  $m$  calculated within SFA. See Sec. III A for more details.

#### B. Intensity of HFM components

We study the behavior of the spectral HFM response starting from the SFA results shown in Fig. 2 for the squared absolute values of the susceptibilities as a function of the number of strong-field photons  $q$  for different numbers of the weak-field photons  $m$ .<sup>3</sup> We can see that the susceptibilities are comparable for different  $q$  lying in the plateau. Moreover, the susceptibilities for the same order  $|m|$  are very close to each other

$$\kappa_q^{(m)} \approx \kappa_q^{(-m)},$$

which agrees with our analytical qsSFA results (17) to (19).

Figure 3 describes the ratio of the susceptibilities for  $m \neq 0$  and  $m = 0$  obtained from SFA [Fig. 3(a)] and TDSE [Fig. 3(b)] calculations. For the first-order processes  $|m| = 1$ , we present the intensity ratio, while for the second-order processes  $|m| = 2$ , we present the ratio of the absolute values; this corresponds to the analytical result for both cases [see Eqs. (17) to (19)] being the same<sup>4</sup>:  $[\frac{U_p}{\mathcal{E}_0 \omega_0} D[t_q, \tau_{\text{st}}(t_q)]]^2$ . Figure 3(a) demonstrates a good agreement of this analytical qsSFA result with the full SFA calculation, except for the cutoff region. The divergence in this region occurs due to inapplicability of the single-trajectory approach used for qsSFA. In turn, in Fig. 3(b) one can see an overall agreement of the TDSE results for the ratio of the susceptibilities with the analytical qsSFA result for the plateau harmonics and again a weaker agreement for the cutoff ones.

In Fig. 4 we present the same ratios but as a function of the fundamental frequency calculated within SFA. These results show a reasonable agreement between SFA and qsSFA approaches for a wide range of frequencies.

<sup>3</sup>We denote as  $m = (0, 2)$  the results related to  $\kappa_q^{(0,2)}$ .

<sup>4</sup>For  $m = (0, 2)$  we present  $|\frac{\kappa_q^{(0,2)}}{2\kappa_q^{(0)}}|$ .

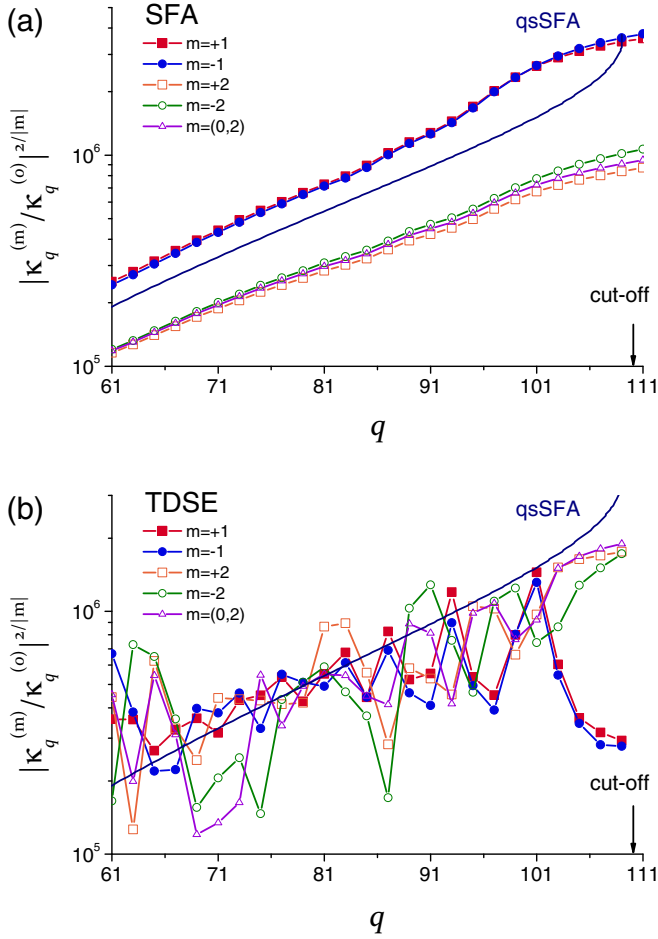


FIG. 3. Ratios of the susceptibilities for  $m \neq 0$  and  $m = 0$  as functions of  $q$ , calculated (a) via SFA and (b) via numerical TDSE solution. The analytical qsSFA result shown by navy solid line for all the ratios is  $\{U_p/(\mathcal{E}_0\omega_0)D[t_q, \tau_{st}(t_q)]\}^2$ .

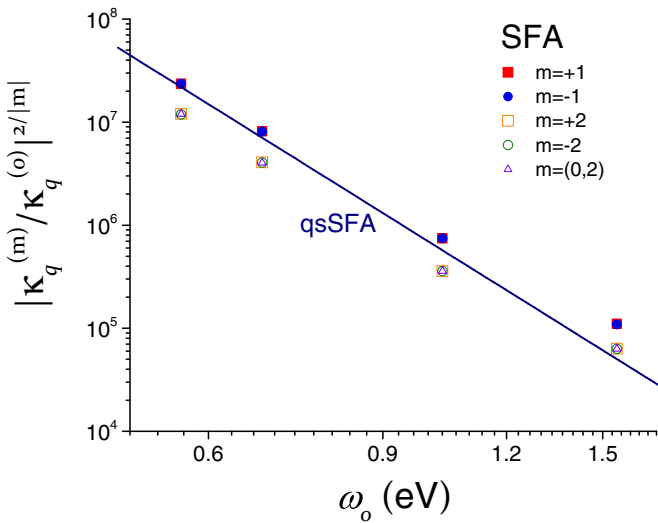


FIG. 4. Susceptibility ratio as functions of the fundamental frequency  $\omega_0$  in log-log scale. These ratios are calculated via SFA for certain plateau harmonic (namely  $q = 31$  for 800 nm,  $q = 85$  for 1200 nm,  $q = 269$  for 1800 nm, and  $q = 461$  for 2200 nm) corresponding to  $D[t_q, \tau_{st}(t_q)] = 2$ .

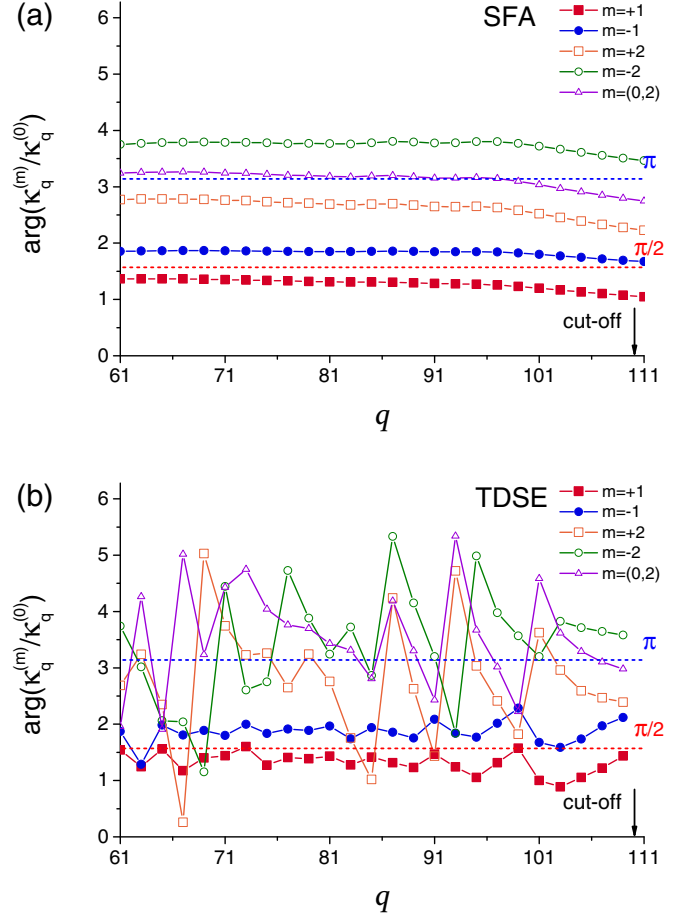


FIG. 5. Arguments of  $\kappa_q^{(m)}/\kappa_q^{(0)}$  as functions of  $q$  calculated via (a) SFA and (b) numerical TDSE solution. The two-color field parameters are the same as in Fig. 3. Equation (17) predicts the argument of  $\pi/2$  for  $|m| = 1$  and Eqs. (18) and (19) predict the argument of  $\pi$  for  $|m| = 2$ .

C. Phase of HFM components

We analyze the behavior of the arguments of the susceptibility ratios as functions of  $q$ , see Fig. 5, calculated via SFA [Fig. 5(a)] and numerical TDSE solution [Fig. 5(b)]. One can see a good agreement between both SFA and TDSE, and qsSFA results for  $|m| = 1$  as well as between SFA and qsSFA results for  $|m| = 2$ . The numerical TDSE results for  $|m| = 2$  are very noisy; however, the average result is still close to the analytical qsSFA prediction, except the cutoff region. The later region performs a deviation discussed above.

IV. HFM IN THE TIME DOMAIN

The difference between the spectral phases of the successive HHG components defines the emission time  $t_q^e = (\varphi_q - \varphi_{q-2})/(2\omega_0)$  for attosecond pulses obtained using a group of harmonics close to the  $q$ th one [31,32,43,44]. The emission time for HHG components grows with increasing harmonic number [45] for plateau harmonics (the so-called harmonic ‘‘attochirp’’) and it is approximately constant for the cutoff ones. It has been also shown that the spectral region of these

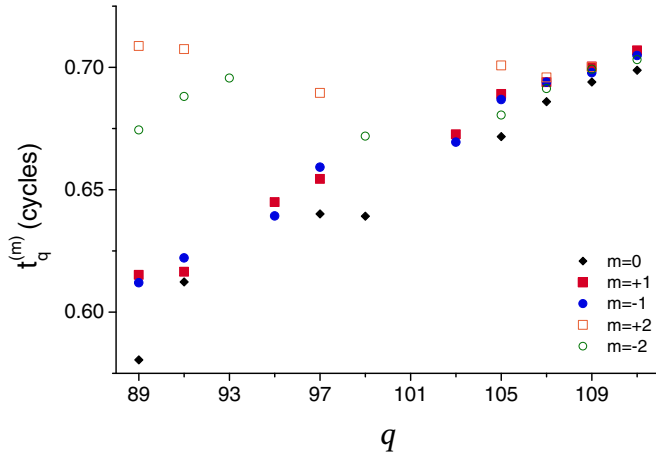


FIG. 6. Emission time (in fundamental cycles) for HHG ( $m = 0$ ) and HFM ( $m \neq 0$ ) components near the cutoff, calculated via Eq. (21) using the TDSE results.

phase-matched harmonics expands with the fundamental frequency [39].

Assuming that the HFM components with certain  $m$  can be selected experimentally (see Sec. VI), below we consider attosecond pulses obtained from a group of HFM components with given  $m$  and different  $q$ . We generalize the concept of the emission time to HFM, where we define it through the phase difference between neighboring HFM components with the same  $m$ :

$$t_q^{(m)} = \frac{\arg(\kappa_q^{(m)}) - \arg(\kappa_{q-2}^{(m)})}{2\omega_0}. \quad (21)$$

Analytical qsSFA (17) to (19) as well as SFA and TDSE results in Fig. 5 show that the phase shift between  $\kappa_q^{(m)}$  with different  $m$  does not depend on  $q$  in the plateau region. This means that the emission time for an attosecond pulse consisting of several HFM components with certain  $m$  and different  $q$  is the same as for the attosecond pulse obtained through the HHG process with corresponding  $q$ . Moreover, the attochirp for these pulses is the same, thus the duration of the attopulses is the same.

However, one can see in Fig. 5 that there is a regular deviation from this behavior in the cutoff region. This deviation corresponds to the emission times shown in Fig. 6, which are calculated using the TDSE results (SFA results demonstrate the same behavior) for HHG and HFM components in this region.<sup>5</sup> From Fig. 6 we see that the spectral region where the HFM emission time does not depend on  $q$  is broader for higher  $m$ . Thus, the components in the cutoff region with higher  $m$  can provide shorter attosecond pulses. Figure 7 presenting the TDSE results (the SFA ones are similar) shows the normalized envelopes of the attosecond pulses obtained from the HFM components with the highest  $q$ . One can see that the attosecond-pulse duration decreases with  $|m|$ .

<sup>5</sup>To exclude numerical noise artifacts, we present only points where  $|\kappa_q^{(m)}|$  and  $|\kappa_{q-2}^{(m)}|$  exceed 10% of the maximal  $|\kappa_q^{(m)}|$  value achieved at  $q = 107$ .

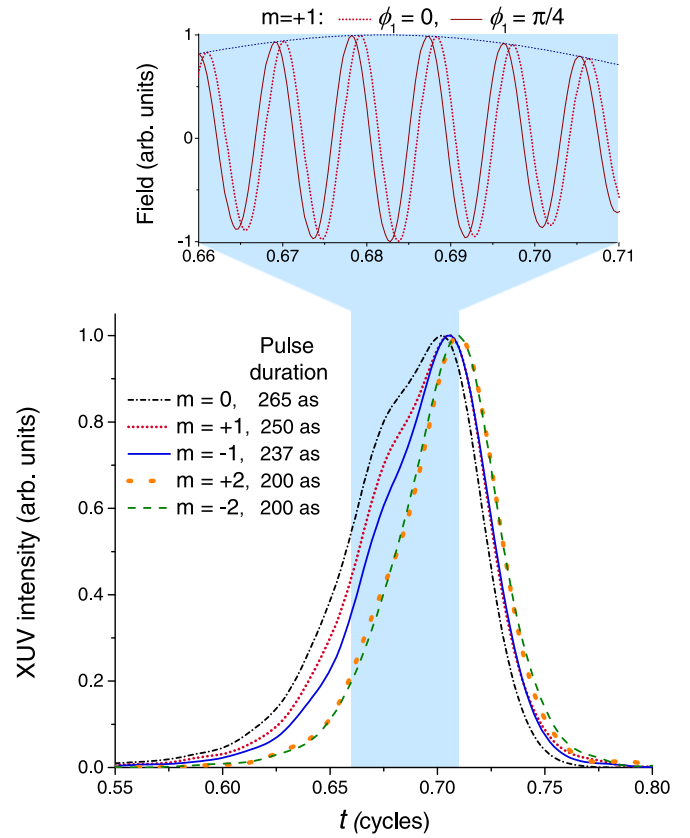


FIG. 7. Normalized envelope of the attosecond pulses obtained via numerical TDSE solution using components with  $q > 100$  and different  $m$ ; the attopulse durations are shown. The inset shows the XUV fields of the attosecond pulses obtained using  $m = +1$  for different phases of the weak field; the XUV field envelope is also shown.

This feature of the cutoff region can be qualitatively explained considering the change of the HHG emission time caused by the quasistatic field within the simple-man approach. It is shown in Fig. 8 that in the presence of the static

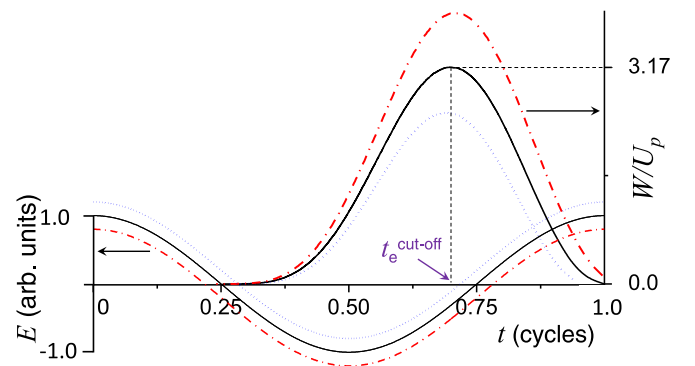


FIG. 8. Total field and kinetic energies of the returning electron calculated via the simple-man model as functions of time for zero quasistatic field (solid black lines) and for quasistatic field “positive” (dotted blue lines) and “negative” (red dash-dotted lines) to the laser field at the half-cycle when the electron is detached.

field there are “above- $3.17 U_p$ ” harmonics generated due to the ionization at the “negative” half-cycle (i.e., when the laser field and the quasistatic field are opposite to each other), as was shown in Ref. [46]. The emission time for these harmonics is close to the emission time for the cutoff harmonics generated in the absence of the static field,  $t_{\text{cutoff}}^e$ . Moreover, for some range of “below- $3.17 U_p$ ” harmonics the emission time is also shifted towards  $t_{\text{cutoff}}^e$  because these harmonics correspond to the cutoff for the emission at the “positive” half-cycle. Thus, the correction of the emission time due to the quasistatic field moves this time towards  $t_{\text{cutoff}}^e$  for both “above- $3.17 U_p$ ” and “below- $3.17 U_p$ ” harmonics. As a result, the emission time of HFM components described by  $\kappa_q^{(\pm 2)}$  is close to  $t_{\text{cutoff}}^e$ .

## V. CEP OF ATTOSECOND PULSES

The CEP of the attosecond pulses obtained via HHG does not depend on the phase of the generating field and depends on other properties of the generating pulse in a complex way [47,48]. However, this phase is of key importance in some applications [49,50]. Here we show that the CEP of the attosecond pulses obtained via HFM can be easily controlled. It is curious to note that a similar CEP variation for femtosecond optical pulses obtained using a comb of frequencies slightly shifted from multiples of a repetition frequency is well known in  $f$ - $2f$  interferometry [35].

The field of the XUV attosecond pulse obtained using  $m$ th order HFM components with complex amplitudes  $\mathcal{E}_q^{(m)}$  is written as

$$\begin{aligned} & \sum_q \mathcal{E}_q^{(m)} \exp(-iq\omega_0 t - im\omega_1 t) \\ & \equiv \mathcal{E}_{\text{XUV}}^{(m)}(t) \exp(-i\Omega t + i\varphi_{\text{CEP}}), \end{aligned} \quad (22)$$

where  $\mathcal{E}_{\text{XUV}}^{(m)}(t)$  is a slowly varying periodic envelope,  $\Omega$  is a carrier frequency and  $\varphi_{\text{CEP}}$  is a CEP. If the phases of the driving fields are changed by phase advances  $\phi_0$  and  $\phi_1$ , the phase of the HFM component changes by  $q\phi_0 + m\phi_1$ ; here it is important to stress, that this is the case for arbitrary field amplitudes [13], so the conclusions of this section are valid beyond the assumptions of weak amplitude and low frequency of the second field. The emission time of the attosecond pulse changes by  $\delta t$ , and its CEP changes by  $\delta\varphi_{\text{CEP}}$ :

$$\begin{aligned} & \sum_q \mathcal{E}_q^{(m)} \exp(-iq\omega_0 t + iq\phi_0 - im\omega_1 t + im\phi_1) \\ & \equiv \mathcal{E}_{\text{XUV}}^{(m)}(t + \delta t) \exp[-i\Omega(t + \delta t) + i\varphi_{\text{CEP}} + i\delta\varphi_{\text{CEP}}]. \end{aligned} \quad (23)$$

Combining Eqs. (22) and (23), one finds

$$\delta t = -\phi_0/\omega_0 \quad (24)$$

and

$$\delta\varphi_{\text{CEP}} = m \left( \phi_1 - \phi_0 \frac{\omega_1}{\omega_0} \right). \quad (25)$$

This conclusion that phase advances of generating fields affect the CEP of the attosecond pulse generated via HFM is demonstrated by our numerical TDSE calculations. The inset

in Fig. 7 shows the fields of the attosecond pulses for  $m = +1$  generated under  $\phi_1 = 0$  and  $\phi_1 = \pi/4$ . One can see that the CEP of the second pulse is shifted by  $\pi/4$ , in agreement with Eq. (25). As a result, by tuning the phase of one of the generating fields, one can control the CEP of the attosecond pulse.

For the attosecond pulses generated via HFM, the CEP varies for the successive pulses in the train, in contrast to the case of HHG. The variation of the CEP from one attosecond pulse to another  $\Delta\varphi_{\text{CEP}}$  can be found by writing the field (22) at the time instant  $t - T_0/2$  as

$$\begin{aligned} & \sum_q \mathcal{E}_q^{(m)} \exp[-iq\omega_0(t - T_0/2) - im\omega_1(t - T_0/2)] \\ & \equiv \sum_q \mathcal{E}_q^{(m)} \exp(-iq\omega_0 t - im\omega_1 t + i\Delta\varphi_{\text{CEP}}), \end{aligned} \quad (26)$$

where  $T_0$  is the fundamental period. From the later equation we have

$$\Delta\varphi_{\text{CEP}} = \begin{cases} m\pi \frac{\omega_1}{\omega_0}, & \text{for odd } m \text{ (even } q), \\ \pi + m\pi \frac{\omega_1}{\omega_0}, & \text{for even } m \text{ (odd } q). \end{cases} \quad (27)$$

One can notice that the change of the fundamental phase  $\phi_0$  by  $\pi$  corresponds to the change of the fundamental field direction to the opposite one, so the CEP of the attosecond pulse should change by  $\pi$  (for even  $m$ ) or by zero (for odd  $m$ ). Let us show that this agrees with the equations above. The change of  $\phi_0$  by  $\pi$  leads to the CEP change according to Eq. (25) by  $\delta\varphi_{\text{CEP}} = -m\pi\omega_1/\omega_0$ . According to Eq. (24) this attosecond pulse is emitted at time  $t + \delta t = t - T_0/2$ , thus the attosecond pulse emitted at time  $t$  is the next pulse in the train. Its CEP defined by Eq. (27) differs by  $\Delta\varphi_{\text{CEP}} = \pi + m\pi(\omega_1/\omega_0)$  or by  $\Delta\varphi_{\text{CEP}} = m\pi(\omega_1/\omega_0)$ . Therefore, the total change of CEP  $\delta\varphi_{\text{CEP}} + \Delta\varphi_{\text{CEP}}$  is equal to 0 or  $\pi$ .

## VI. DISCUSSION

The HFM microscopic response for  $m \neq 0$  is lower than the nonlinear microscopic response for HHG, at least within the fields  $\mathcal{E}_1 < \mathcal{E}_1^{\text{th}}$  considered here. However, the macroscopic response for HFM with  $m < 0$  can be much higher due to significantly better phase matching [26]. This takes place for a certain frequency ratio of the generating fields and a certain  $m$ , defined by this ratio. Thus, the phase matching should provide high generation efficiency in conjunction with selection of the HFM components with desired  $m$ . The investigation of the macroscopic HFM properties is a natural outlook of the present study.

There is another approach to separate the HFM components with different  $m$  based on the use of noncoaxial generating beams [11,18]. If the weak field propagates at an angle  $\theta$  to the direction of the laser field, then for  $|m| \ll q$  the HFM component is generated at the angle  $\theta_q^{(m)} = mk_1 \sin \theta / (qk_0 + mk_1 \cos \theta)$ , where  $k_0$  and  $k_1$  are the wave vectors of the generating fields. From the later equation we can obtain that  $|\frac{\partial}{\partial q} \theta_q^{(m)}| \ll |\frac{\partial}{\partial m} \theta_q^{(m)}|$ . Thus, selecting a certain range of  $q$  with a frequency filter, we have the HFM components with different  $m$  propagating in significantly different directions, while the ones with the same  $m$  propagate in similar directions (similar enough that the difference between

these directions can be less than the beam divergence). As a result, the HFM components with the desired  $m$  can be selected with a spatial filter such as a slit. Moreover, the HFM components with negative  $m$  (effectively generated due to better phase matching) are emitted in a direction different from the directions of the generating beams. This makes detection and utilization of this radiation more convenient. Finally, the focusing properties of the XUV can be used to select the chosen HFM components. It was shown [43,51–53] that high harmonics can be generated as focused beams, and that focusing properties of the beams with similar  $q$  are similar to each other. HFM components generated via two (coaxial) beams with different focusing properties can be used to obtain focused HFM beams for certain  $m$ . The focusing properties of the HFM components in this case can be found similarly to the propagation directions of the components in the case of noncoaxial generation. After focusing HFM components with certain  $m$ , the undesired remainder of HHG and HFM signals can be suppressed by a spatial filter, for instance, with an iris.

HFM paves a way to the generation of a single attosecond pulse with controllable CEP. Namely, if the laser field provides some gating for attosecond pulse generation (such as ellipticity gating [54] or attosecond lighthouse [55]), this allows for isolated attosecond pulse generation. The phase variation of the weak generating field would not affect the gating properties, but it would provide CEP control for the generated single attosecond pulse.

## VII. CONCLUSION

We investigate theoretically the single-atom properties of the HFM process for the case of a strong laser field combined with a weaker low-frequency one. Using SFA theory we consider the later field as a quasistatic one, and assume

that the main role of this field is to produce a correction of the action accumulated by the electron during its free motion. Within this assumption we show that the amplitudes of HFM spectral components generated by  $q$  fundamental photons and  $m$  low-frequency photons ( $|m| \leq 2$  are considered) can be written as a product of the  $q$ th high-harmonic amplitude, the  $|m|$ th power of the weak field amplitude, and a multiplier which increases with  $\tau$  (the time of the electronic free motion) and rapidly decreases with the fundamental frequency, see Eqs. (15) to (19). We show that the HFM components are shifted in phase by  $|m|\pi/2$  with respect to high harmonics. For  $q$  lying in the plateau region these analytical results agree with numerically integrated SFA, as well as with numerical TDSE simulations, while for the cutoff region there is a regular deviation.

This deviation describes the spectral region of attochirp-free HFM components which is broader than the one for HHG. We discuss the origin of this feature of the cutoff HFM components and demonstrate that it leads to shorter durations of attosecond pulses obtained via HFM, and that the duration decreases with an increase of  $|m|$ . Moreover, we show that the CEP of the attosecond pulses obtained via HFM can be easily controlled by tuning the phases of the generating fields, while such control is impossible for the pulses obtained via HHG. The equations describing the attosecond pulse CEP are applicable even beyond the assumption of weakness and low frequency of the second field. Finally, we would like to stress that due to perspective of phase-matched generation for long propagation distances, HFM can substantially improve the efficiency of the attosecond pulse sources.

## ACKNOWLEDGMENTS

This study was funded by RSF (Grant No. 22-22-00242).

- 
- [1] P. B. Corkum and F. Krausz, Attosecond science, *Nat. Phys.* **3**, 381 (2007).
  - [2] F. Krausz and M. Ivanov, Attosecond physics, *Rev. Mod. Phys.* **81**, 163 (2009).
  - [3] D. M. Villeneuve, Attosecond science, *Contemp. Phys.* **59**, 47 (2018).
  - [4] M. Y. Ryabikin, M. Y. Emelin, and V. V. Strelkov, Attosecond electromagnetic pulses: Generation, measurement, and application. attosecond metrology and spectroscopy, *Phys. Usp.* (2022), doi: 10.3367/UFNe.2021.10.039078
  - [5] A. S. Johnson, D. Wood, D. R. Austin, C. Brahm, A. Gregory, K. B. Holzner, S. Jarosch, E. W. Larsen, S. Parker, C. Strüber, P. Ye, J. W. G. Tisch, and J. P. Marangos, Apparatus for soft x-ray table-top high harmonic generation, *Rev. Sci. Instrum.* **89**, 083110 (2018).
  - [6] T. Gaumnitz, A. Jain, Y. Pertot, M. Huppert, I. Jordan, F. Ardana-Lamas, and H. J. Wörner, Streaking of 43-attosecond soft-X-ray pulses generated by a passively CEP-stable mid-infrared driver, *Opt. Express* **25**, 27506 (2017).
  - [7] J. Li, J. Lu, A. Chew, S. Han, J. Li, Y. Wu, H. Wang, S. Ghimire, and Z. Chang, Attosecond science based on high harmonic generation from gases and solids, *Nat. Commun.* **11**, 2748 (2020).
  - [8] P. Ye, T. Csizmadia, L. G. Oldal, H. N. Gopalakrishna, M. Füle, Z. Filus, B. Nagyillés, Z. Divéki, T. Grósz, M. Dumergue, P. Jójárt, I. Seres, Z. Bengery, V. Zuba, Z. Várallyay, B. Major, F. Frassetto, M. Devetta, G. D. Lucarelli, M. Lucchini *et al.*, Attosecond pulse generation at ELI-ALPS 100 kHz repetition rate beamline, *J. Phys. B: At. Mol. Opt. Phys.* **53**, 154004 (2020).
  - [9] H. Eichmann, A. Egbert, S. Nolte, C. Momma, B. Wellegehausen, W. Becker, S. Long, and J. K. McIver, Polarization-dependent high-order two-color mixing, *Phys. Rev. A* **51**, R3414(R) (1995).
  - [10] O. Cohen, T. Popmintchev, D. M. Gaudiosi, M. M. Murnane, and H. C. Kapteyn, Unified Microscopic-Macroscopic Formulation of High-Order Difference-Frequency Mixing in Plasmas, *Phys. Rev. Lett.* **98**, 043903 (2007).
  - [11] J. B. Bertrand, H. J. Wörner, H.-C. Bandulet, E. Bisson, M. Spanner, J.-C. Kieffer, D. M. Villeneuve, and P. B. Corkum, Ultrahigh-Order Wave Mixing in Noncollinear High Harmonic Generation, *Phys. Rev. Lett.* **106**, 023001 (2011).
  - [12] Y. Oguchi, S. Minemoto, and H. Sakai, Generation of high-order sum and difference frequencies by adding an intense



- parallel- and perpendicular-polarized infrared laser field, *Phys. Rev. A* **80**, 021804(R) (2009).
- [13] V. V. Strelkov, High-order optical processes in intense laser field: Towards nonperturbative nonlinear optics, *Phys. Rev. A* **93**, 053812 (2016).
- [14] R. A. Ganeev, High-order sum and difference frequency generation using tunable two- and three-color commensurate and incommensurate mid-infrared pumps of graphite plasma, *J. Opt. Soc. Am. B* **33**, E93 (2016).
- [15] J. L. Ellis, K. M. Dorney, C. G. Durfee, C. Hernández-García, F. Dollar, C. A. Mancuso, T. Fan, D. Zusin, C. Gentry, P. Grychtol, H. C. Kapteyn, M. M. Murnane, and D. D. Hickstein, Phase matching of noncollinear sum and difference frequency high harmonic generation above and below the critical ionization level, *Opt. Express* **25**, 10126 (2017).
- [16] K. A. Tran, K. B. Dinh, P. Hannaford, and L. V. Dao, Phase-matched nonlinear wave-mixing processes in xuv region with multicolor lasers, *Appl. Opt.* **58**, 2540 (2019).
- [17] N. Harkema, A. Plunkett, and A. Sandhu, Tunable high-order frequency mixing for xuv transient absorption and photoelectron spectroscopies, *Opt. Express* **27**, 31053 (2019).
- [18] C. Chappuis, D. Bresteau, T. Auguste, O. Gobert, and T. Ruchon, High-order harmonic generation in an active grating, *Phys. Rev. A* **99**, 033806 (2019).
- [19] S. Jiang, M. Kowalewski, and K. E. Dorfman, Multi-wave mixing in the high harmonic regime: Monitoring electronic dynamics, *Opt. Express* **29**, 4746 (2021).
- [20] E. Constant, D. Garzella, P. Breger, E. Mével, C. Dorrer, C. Le Blanc, F. Salin, and P. Agostini, Optimizing High Harmonic Generation in Absorbing Gases: Model and Experiment, *Phys. Rev. Lett.* **82**, 1668 (1999).
- [21] P. L. Shkolnikov, A. E. Kaplan, and A. Lago, Phase matching for large-scale frequency upconversion in plasma, *Opt. Lett.* **18**, 1700 (1993).
- [22] S. Meyer, H. Eichmann, T. Menzel, S. Nolte, B. Wellegehausen, B. N. Chichkov, and C. Momma, Phase-Matched High-Order Difference-Frequency Mixing in Plasmas, *Phys. Rev. Lett.* **76**, 3336 (1996).
- [23] A. V. Birulin, V. T. Platonenko, and V. V. Strelkov, High-harmonic generation in interfering waves, *J. Exp. Theor. Phys* **83**, 33 (1996).
- [24] S. Meyer, B. N. Chichkov, B. Wellegehausen, and A. Sanpera, Phase-matched high-order harmonic generation and parametric amplification, *Phys. Rev. A* **61**, 063811 (2000).
- [25] C. M. Heyl, P. Rudawski, F. Brizuela, S. N. Bengtsson, J. Mauritsson, and A. L'Huillier, Macroscopic Effects in Non-collinear High-Order Harmonic Generation, *Phys. Rev. Lett.* **112**, 143902 (2014).
- [26] M. A. Khokhlova and V. V. Strelkov, Highly efficient XUV generation via high-order frequency mixing, *New J. Phys.* **22**, 093030 (2020).
- [27] O. Hort, A. Dubrouil, M. A. Khokhlova, D. Descamps, S. Petit, F. Burgy, E. Mével, E. Constant, and V. V. Strelkov, High-order parametric generation of coherent XUV radiation, *Opt. Express* **29**, 5982 (2021).
- [28] M. Lewenstein, Ph. Balcou, M. Yu. Ivanov, A. L'Huillier, and P. B. Corkum, Theory of high-harmonic generation by low-frequency laser fields, *Phys. Rev. A* **49**, 2117 (1994).
- [29] M. B. Gaarde, A. L'Huillier, and M. Lewenstein, Theory of high-order sum and difference frequency mixing in a strong bichromatic laser field, *Phys. Rev. A* **54**, 4236 (1996).
- [30] M. Lewenstein, P. Salières, and A. L'Huillier, Phase of the atomic polarization in high-order harmonic generation, *Phys. Rev. A* **52**, 4747 (1995).
- [31] P. Antoine, A. L'Huillier, and M. Lewenstein, Attosecond Pulse Trains Using High-Order Harmonics, *Phys. Rev. Lett.* **77**, 1234 (1996).
- [32] Y. Mairesse, A. de Bohan, L. J. Frasinski, H. Merdji, L. C. Dinu, P. Monchicourt, P. Breger, M. Kovačev, R. Taïeb, B. Carré, H. G. Muller, P. Agostini, and P. Salières, Attosecond Synchronization of High-Harmonic Soft X-rays, *Science* **302**, 1540 (2003).
- [33] M. C. Kohler, C. H. Keitel, and K. Z. Hatsagortsyan, Attochirp-free high-order harmonic generation, *Opt. Express* **19**, 4411 (2011).
- [34] V. V. Strelkov, Attosecond-pulse production using resonantly enhanced high-order harmonics, *Phys. Rev. A* **94**, 063420 (2016).
- [35] R. Paschotta, Carrier-envelope offset, CEO frequency, CEP, absolute phase, Encyclopedia of laser physics and technology, Retrieved 5 May 2015.
- [36] P. B. Corkum, Plasma Perspective on Strong Field Multiphoton Ionization, *Phys. Rev. Lett.* **71**, 1994 (1993).
- [37] K. J. Schafer, B. Yang, L. F. DiMauro, and K. C. Kulander, Above Threshold Ionization Beyond the High Harmonic Cutoff, *Phys. Rev. Lett.* **70**, 1599 (1993).
- [38] M. Bertolino and J. M. Dahlström, Multiphoton interaction phase shifts in attosecond science, *Phys. Rev. Research* **3**, 013270 (2021).
- [39] M. A. Khokhlova and V. V. Strelkov, Phase properties of the cutoff high-order harmonics, *Phys. Rev. A* **93**, 043416 (2016).
- [40] E. Pisanty, RB-SFA: High Harmonic Generation in the Strong Field Approximation via Mathematica, GitHub, <https://github.com/episanty/RB-SFA>, (2020).
- [41] V. V. Strelkov, A. F. Sterjantov, N. Y. Shubin, and V. T. Platonenko, XUV generation with several-cycle laser pulse in barrier-suppression regime, *J. Phys. B: At. Mol. Opt. Phys.* **39**, 577 (2006).
- [42] V. V. Strelkov, V. T. Platonenko, and A. Becker, High-harmonic generation in a dense medium, *Phys. Rev. A* **71**, 053808 (2005).
- [43] V. T. Platonenko and V. V. Strelkov, Spatiotemporal structure of the combined field of high-order harmonics and generation of attosecond pulses, *Quantum Electron.* **27**, 779 (1997).
- [44] K. Varjú, Y. Mairesse, B. Carré, M. B. Gaarde, P. Johnsson, S. Kazamias, R. López-Martens, J. Mauritsson, K. J. Schafer, P. H. Balcou, A. L'Huillier, and P. Salières, Frequency chirp of harmonic and attosecond pulses, *J. Mod. Opt.* **52**, 379 (2005).
- [45] K. L. Ishikawa, High-harmonic generation, in *Advances in Solid State Lasers*, edited by M. Grishin (IntechOpen, Rijeka, Croatia, 2010), Chap. 19.
- [46] V. D. Taranukhin and N. Y. Shubin, High-order harmonic generation by the atoms in strong bichromatic fields, *Quantum Electron.* **29**, 638 (1999).
- [47] C. Guo, A. Harth, S. Carlström, Y.-C. Cheng, S. Mikaelsson, E. Mårzell, C. Heyl, M. Miranda, M. Gisselbrecht, M. B. Gaarde, K. J. Schafer, A. Mikkelsen, J. Mauritsson, C. L. Arnold, and

- A. L'Huillier, Phase control of attosecond pulses in a train, *J. Phys. B: At. Mol. Opt. Phys.* **51**, 034006 (2018).
- [48] G. Sansone, E. Benedetti, F. Calegari, C. Vozzi, L. Avaldi, R. Flammini, L. Poletto, P. Villoresi, C. Altucci, R. Velotta, S. Stagira, S. De Silvestri, and M. Nisoli, Isolated single-cycle attosecond pulses, *Science* **314**, 443 (2006).
- [49] L.-Y. Peng and A. F. Starace, Attosecond pulse carrier-envelope phase effects on ionized electron momentum and energy distributions, *Phys. Rev. A* **76**, 043401 (2007).
- [50] J. M. Ngoko Djiokap, S. X. Hu, W.-C. Jiang, L.-Y. Peng, and A. F. Starace, Asymmetries in production of  $\text{he}^+(n = 2)$  with an intense few-cycle attosecond pulse, *Phys. Rev. A* **88**, 011401(R) (2013).
- [51] E. Frumker, G. G. Paulus, H. Niikura, A. Naumov, D. M. Villeneuve, and P. B. Corkum, Order-dependent structure of high harmonic wavefronts, *Opt. Express* **20**, 13870 (2012).
- [52] L. Quintard, V. Strelkov, J. Vabek, O. Hort, A. Dubrouil, D. Descamps, F. Burgy, C. Péjot, E. Mével, F. Catoire, and E. Constant, Optics-less focusing of xuv high-order harmonics, *Sci. Adv.* **5**, eaau7175 (2019).
- [53] K. Veyrinas, J. Vábek, C. Valentin, D. Descamps, C. Péjot, F. Burgy, E. Constant, E. Mével, and F. Catoire, Spectral filtering of high-order harmonics via optics-free focusing, *Opt. Express* **29**, 29813 (2021).
- [54] I. J. Sola, E. Mével, L. Elouga, E. Constant, V. Strelkov, L. Poletto, P. Villoresi, E. Benedetti, J.-P. Caumes, S. Stagira, C. Vozzi, G. Sansone, and M. Nisoli, Controlling attosecond electron dynamics by phase-stabilized polarization gating, *Nat. Phys.* **2**, 319 (2006).
- [55] H. Vincenti and F. Quéré, Attosecond Lighthouses: How To Use Spatiotemporally Coupled Light Fields To Generate Isolated Attosecond Pulses, *Phys. Rev. Lett.* **108**, 113904 (2012).